HYDROSTATIC ADJUSTMENT IN VERTICALLY STRATIFIED ATMOSPHERES

Dean G. Duffy

Code 912
NASA/Goddard Space Flight Center
Greenbelt, MD 20771

May 2000

Submitted to *Journal of the Atmospheric Sciences*

Abstract

Hydrostatic adjustment due to diabatic heating in two nonisothermal atmospheres is examined. In the first case the temperature stratification is continuous; in the second case the atmosphere is composed of a warm, isothermal troposphere and a colder, isothermal, semi-infinitely deep stratosphere. In both cases hydrostatic adjustment, to a good approximation, follows the pattern found in the Lamb problem (semi-infinitely deep, isothermal atmosphere): Initially we have acoustic waves with the kinetic energy increasing or decreasing at the expense of available elastic energy. After this initial period the acoustic waves evolve into acoustic-gravity waves with the kinetic, available potential and available elastic energies interacting with each other. Relaxation to hydrostatic balance occurs within a few oscillations.

Stratification in an atmosphere with a continuous temperature profile affects primarily the shape and amplitude of the disturbances. In the two-layer atmosphere, a certain amount of energy is trapped in the tropospheric waveguide as disturbances reflect off the tropopause and back into the troposphere. With each internal reflection a portion of this trapped energy escapes and radiates to infinity.

1. Introduction.

The atmosphere continuously undergoes various forms of adjustment. On the large scales baroclinic waves are excited and reduce the north-south temperature gradient so efficiently that the extratropical atmosphere remains near neutral stability (Stone 1978). Inertial-gravity waves radiate ageostrophic disturbances out to infinity, leaving behind a geostrophic final state (Rossby 1938). On the mesoscale hydrostatic imbalances are eliminated by the excitation of acoustic-gravity waves.

Although baroclinic and geostrophic adjustment have received considerable attention, it is only recently that hydrostatic adjustment has been studied. Bannon (1995) examined how hydrostatic imbalances excite acoustic-gravity waves in an isothermal atmosphere, the so-called Lamb problem. An important aspect of his analysis was a computation of the energetics. Bannon showed that nonhydrostatic disturbances may generate three types of energy: kinetic, available potential and available elastic energies. Although he found the initial and final distribution of these three energies during hydrostatic adjustment, he did not follow their temporal evaluation. We will do this in Section 2.

Although Lamb's problem provides many useful insights into hydrostatic adjustment, the atmosphere is not isothermal. Vertical stratification plays an important role in determining the vertical propagation of acoustic-gravity waves from their origin in the troposphere into the upper atmosphere (Francis 1973, Friedman 1962). Consequently, vertical stratification must also play an important role in hydrostatic adjustment. The purpose of this paper is to examine those effects.

To realize our goal, I have examined two stratifications which highlight different effects. In Section 3, we examine hydrostatic adjustment when the temperature profile is given by $T_0(z) = T_*\,(1 + \beta e^{-z/D})$. This basic state yields a nearly constant lapse rate in the troposphere and an essentially isothermal stratosphere; a similar model was examined by Pekeris (1948). With this thermal stratification, acoustic-gravity waves travel at different phase speeds within the atmosphere, just as electric waves do within a nonuniform transmission line.

To examine the case when a sharp troposphere is present, we introduce in Section 4 a two-layer atmosphere where one layer represents the troposphere and the other models the stratosphere. Both layers are isothermal but at different temperatures. In this case acoustic-gravity waves will reflect at the interface

(tropopause) and energy leaks from the troposphere into the stratosphere. Finally, in Section 5 we present our conclusions.

2. The Lamb Problem

As a benchmark for later computations we first examine the energetics during hydrostatic adjustment in an isothermal atmosphere. The hydrostatic adjustment arises due to diabatic heating of finite vertical extent.

We begin by modeling the atmosphere as a stably stratified, inviscid, diatomic, ideal gas in a Cartesian coordinate system where $-g\mathbf{k}$ equals the acceleration due to gravity. The one-dimensional linearized equations for small-amplitude perturbations about the basic state

$$\begin{aligned} \rho_0(z) &= \rho_* e^{-z/H_S}, \qquad & p_0(z) &= p_* e^{-z/H_S}, \\ T_0(z) &= T_*, & \theta_0(z) &= T_* e^{\kappa z/H_S} \end{aligned} \tag{2.1}$$

are

$$\rho_0 \frac{\partial w}{\partial t} = -\frac{\partial p}{\partial z} - \rho g. \tag{2.2}$$

$$\rho_0 \frac{\partial \rho}{\partial t} + \frac{d\rho_0}{dz} w + \rho_0 \frac{\partial w}{\partial z} = 0. \tag{2.3}$$

$$\frac{\partial p}{\partial t} + \rho_0 c^2 \frac{\partial w}{\partial z} - \rho_0 g w = \Delta p [H(z-a) - H(z-2a)]\delta(t). \tag{2.4}$$

and

$$\frac{\partial \theta}{\partial t} + \frac{d\theta_0}{dz} w = \frac{\theta_0 \Delta p}{\gamma p_0} [H(z-a) - H(z-2a)]\delta(t). \tag{2.5}$$

where the basic state quantities have a subscript nought and the asterisk subscript denotes a constant reference value. Here w denotes the velocity in the vertical z direction at time t, p denotes pressure, T denotes the temperature, θ denotes the potential temperature, ρ denotes the density, H_S, the scale height, equals RT_*/g, R denotes the ideal gas constant, $\gamma = C_p/C_v = 7/5$ is the ratio of the specific heats at constant pressure and volume, $c^2 = \gamma RT_*$ and $\kappa = (\gamma - 1)/\gamma$. The functions $H(\ )$ and $\delta(\ )$ denote the Heaviside step and delta functions, respectively. In addition to the governing equations, we have the boundary conditions that

$$w(0,t) = 0 \qquad \text{and} \qquad \lim_{z \to \infty} \rho_0(z) w^2(z,t) \to 0 \tag{2.6}$$

and the initial conditions that

$$p(z,0) = \theta(z,0) = \rho(z,0) = w(z,0) = 0. \tag{2.7}$$

Equations (2.2)–(2.5) may be combined together to yield

$$\frac{\partial}{\partial t}\left[\frac{\rho_0 w^2}{2} + \frac{p^2}{2\rho_0 c^2} + \frac{\rho_0}{2N_0^2}\left(\frac{g\theta}{\theta_0}\right)^2\right] = -\frac{\partial(pw)}{\partial z}, \tag{2.8}$$

where

$$N_0^2 = \frac{g}{\theta_0}\frac{\partial \theta_0}{\partial z} = \frac{g\kappa}{H_S}. \tag{2.9}$$

Equation (2.8) describes the energetics of the model; the first term on the left side of (2.8) gives the kinetic energy per unit volume while the second and third terms give the available elastic and available potential energies, respectively. See Bannon (1995).

To solve (2.2)–(2.5), we combine these equations together to obtain a single equation in w:

$$\frac{\partial^2 w}{\partial t^2} + g\gamma\frac{\partial w}{\partial z} - c^2\frac{\partial^2 w}{\partial z^2} = -\frac{\Delta p}{\rho_0}[\delta(z-a) - \delta(z-2a)]\delta(t). \tag{2.10}$$

In appendix A, I solve (2.10) by Fourier sine and Laplace transforms. Once $w(z,t)$ is known, the other solutions follow from (2.3)–(2.5). These solutions are

$$\frac{w(z,t)}{\Delta w} = \tfrac{1}{2}e^{a/H_S}\left[W(|z-2a|,t) - W(z+2a,t)\right] - \tfrac{1}{2}e^{a/2H_S}\left[W(|z-a|,t) - W(z+a,t)\right], \tag{2.11}$$

$$\begin{aligned}\frac{p(z,t)}{\Delta p} &= H(z-a) - H(z-2a) \\ &+ \tfrac{1}{2}e^{a/H_S}e^{-z/2H_S}\left[P(|z-2a|,t) - P(z+2a,t)\right] \\ &- \tfrac{1}{2}e^{a/2H_S}e^{-z/2H_S}\left[P(|z-a|,t) - P(z+a,t)\right] \\ &- \frac{(\gamma-2)ae^{a/H_S}e^{-z/2H_S}}{4\gamma H_S}\left[\Theta(|z-2a|,t) - \Theta(z+2a,t)\right] \\ &+ \frac{(\gamma-2)ae^{a/2H_S}e^{-z/2H_S}}{4\gamma H_S}\left[\Theta(|z-a|,t) - \Theta(z+a,t)\right]\end{aligned} \tag{2.11}$$

and

$$\begin{aligned}\frac{\theta(z,t)}{\Delta T} &= e^{(1+\kappa)z/H_S}\left[H(z-a) - H(z-2a)\right]/\gamma \\ &- \frac{\kappa a e^{a/H_S}e^{(1+2\kappa)z/2H_S}}{2\gamma H_S}\left[\Theta(|z-2a|,t) - \Theta(z+2a,t)\right] \\ &+ \frac{\kappa a e^{a/2H_S}e^{(1+2\kappa)z/2H_S}}{2\gamma H_S}\left[\Theta(|z-a|,t) - \Theta(z+a,t)\right].\end{aligned} \tag{2.12}$$

where

$$W(\xi,t) = e^{z/2H_S} J_0\left[\sqrt{c^2t^2-\xi^2}/(2H_S)\right] H(ct-\xi), \tag{2.13}$$

$$P(\xi,t) = H(ct-\xi)\,\mathrm{sgn}(\xi)\left\{1 - \frac{c\xi}{2H_S}\int_{\xi/c}^{t} \frac{J_1\left[\sqrt{c^2\tau^2-\xi^2}/(2H_S)\right]}{\sqrt{c^2\tau^2-\xi^2}}\,d\tau\right\}. \tag{2.14}$$

and

$$\Theta(\xi,t) = \frac{c\,H(ct-\xi)}{a}\int_{\xi/c}^{t} J_0\left[\sqrt{c^2\tau^2-\xi^2}/(2H_S)\right]\,d\tau. \tag{2.15}$$

$\Delta T = T_0\Delta p/p_*$, $\Delta w = \Delta p/\rho_* c$, sgn( ) is the sign function and J_0( ) and J_1( ) denote Bessel functions of the first kind and zeroth and first order, respectively. The integrals in (2.14)–(2.15) were evaluated using Cote's sixth order scheme (see Fröberg 1968, p. 201).

For a fixed value of a/H_S, $p(z,t)$, $w(z,t)$, and $\theta(z,t)$ may be computed. Initially waves are excited. As these disturbances propagate out to infinity, the atmosphere approaches the steady-state given by

$$w_s(z) = 0, \tag{2.16}$$

$$\begin{aligned}\frac{p_s(z)}{\Delta p} &= H(z-a) - H(z-2a)\\ &+ \tfrac{1}{2}e^{a/H_S}e^{-z/2H_S}\left[\mathrm{sgn}(z-2a)e^{-|z-2a|/2H_S} - e^{-(z+2a)/2H_S}\right]\\ &- \tfrac{1}{2}e^{a/2H_S}e^{-z/2H_S}\left[\mathrm{sgn}(z-a)e^{-|z-a|/2H_S} - e^{-(z+a)/2H_S}\right]\\ &- \frac{(\gamma-2)e^{a/H_S}e^{-z/2H_S}}{2\gamma}\left[e^{-|z-2a|/2H_S} - e^{-(z+2a)/2H_S}\right]\\ &+ \frac{(\gamma-2)e^{a/2H_S}e^{-z/2H_S}}{2\gamma}\left[e^{-|z-a|/2H_S} - e^{-(z+a)/2H_S}\right]\end{aligned} \tag{2.17}$$

and

$$\begin{aligned}\frac{\theta_s(z)}{\Delta T} &= e^{(1+\kappa)z/H_S}[H(z-a) - H(z-2a)]/\gamma\\ &- \frac{\kappa e^{a/H_S}e^{(1+2\kappa)z/2H_S}}{\gamma}\left[e^{-|z-2a|/2H_S} - e^{-(z+2a)/2H_S}\right]\\ &+ \frac{\kappa e^{a/2H_S}e^{(1+2\kappa)z/2H_S}}{\gamma}\left[e^{-|z-a|/2H_S} - e^{-(z+a)/2H_S}\right].\end{aligned} \tag{2.18}$$

Although we could present the temporal evolution of these fields, we have chosen to proceed along a different path. From (2.8), we have that

$$\int_0^\infty \left[\frac{\rho_0 w^2}{2} + \frac{p^2}{2\rho_0 c^2} + \frac{\rho_0}{2N_0^2}\left(\frac{g\theta}{\theta_0}\right)^2\right] dz = \text{ a constant}. \tag{2.19}$$

Consequently, I have graphed in Fig. 1 the temporal evolution of the kinetic (KE), available elastic (AE), and available potential (PE) energies over the entire column. To highlight the transient disturbances, the steady-state values AE and PE have been subtracted off and the plotted energies have been normalized with respect to the total energy.

As Fig. 1 shows, the kinetic energy initially increases (decreases) at the expense (gain) of elastic energy. During this period of time, which depends on a/H_S, we have acoustic waves. After this initial period these acoustic waves evolve into acoustic-gravity waves and hydrostatic adjustment begins to occur. The ebb and flow of energy between AE, KE and PE dampens out with the oscillations having a decreasing period that depends upon a/H_S. Within a few oscillations hydrostatic adjustment has occurred.

We also note that the amount of transient available potential energy is small compared to the transient kinetic and available elastic energies. This is clearly seen in a plot of the integrand of (2.19) presented in Fig. 2. For the available potential energy, essentially all of the energy is given by the steady state (the spike on the left side). In contrast, the kinetic and available elastic energies are dominated by transients that propagate out to infinity.

Having presented the temporal evolution of kinetic, available elastic, and available potential energies during the hydrostatic adjustment problem for the classic Lamb problem, we examine the same problem in the next section where the temperature decreases with height as $T_* \left(1 + \beta e^{-z/D}\right)$.

3. The Exponential Temperature Profile

Having found the waves excited in an uniform (isothermal) atmosphere by a region of diabatic heating, we now examine a continuously varying temperature field, namely

$$T_0(z) = T_* \left(1 + \beta e^{-z/D}\right). \tag{3.1}$$

This particular temperature profile produces a constant lapse rate in the lower troposphere ($z \ll D$) and an isothermal atmosphere in the upper stratosphere ($z \gg D$). Furthermore, the speed of sound decreases monotonically from its maximum at the ground to its minimum value $c_*^2 = \gamma R T_*$ in the upper stratosphere. For the observed atmosphere, $\beta = 0.3$ and $T_* = 220$K. With these particular values for β and T_* and

$a/D = 1.5$. (3.1) yields a surface temperature of 286 K and temperatures of 259 K and 243 K at the heights of 5 km and 10 km, respectively.

Our analysis again starts with (2.2)–(2.5). Again these equations may be combined together to give (2.10) with the exception that now the basic state varies according to (3.1).

$$p_0(z) = p_* e^{-z/H_S} \left(\frac{1+\beta}{1+\beta e^{-z/D}} \right)^{D/H_S}. \tag{3.2}$$

$$\rho_0(z) = \rho_* e^{-z/H_S} \frac{(1+\beta)^{D/H_S}}{(1+\beta e^{-z/D})^{1+D/H_S}}. \tag{3.3}$$

and

$$\theta_0(z) = T_* e^{\kappa z/H_S} \frac{(1+\beta e^{-z/D})^{1+\kappa D/H_S}}{(1+\beta)^{\kappa D/H_S}}. \tag{3.4}$$

where $p_* = \rho_* R T_*$ and p_* is the pressure at $z = 0$. For a statically stable atmosphere, $D/H_S > \beta/\kappa$.

The nondimensional, Laplace-transformed vertical velocity equation becomes

$$\left(1+\beta e^{-az/D}\right) \frac{d^2W}{dz^2} - \frac{a}{H_S}\frac{dW}{dz} - s^2 W = \frac{\rho_*}{\rho_0}[\delta(z-1) - \delta(z-2)]. \tag{3.5}$$

In Appendix B I solve (3.5). In terms of the nondimensional z, $W(z,s)$ is

$$\begin{aligned} W(z,s) = {} & \frac{\rho_* \exp[(z-2)a/(2H_S)]}{2\rho_0(2a)(1+\beta e^{-2a/D})^{1+D/H_S}\sqrt{s^2+a^2/4H_S^2}} \quad \frac{F(a',b';c';\zeta)}{F(a',b';c';-\beta)} \\ & \times \left\{ F(a',b';c';-\beta) F(1+a'-c', 1+b'-c'; 2-c'; u) \exp\left[(z-2)\sqrt{s^2+a^2/4H_S^2}\right] \right. \\ & \left. - F(a',b';c';u) F(1+a'-c', 1+b'-c'; 2-c'; -\beta) \exp\left[-(z+2)\sqrt{s^2+a^2/4H_S^2}\right] \right\} \\ & - \frac{\rho_* \exp[(z-1)a/(2H_S)]}{2\rho_0(a)(1+\beta e^{-a/D})^{1+D/H_S}\sqrt{s^2+a^2/4H_S^2}} \quad \frac{F(a',b';c';\zeta)}{F(a',b';c';-\beta)} \\ & \times \left\{ F(a',b';c';-\beta) F(1+a'-c', 1+b'-c'; 2-c'; u) \exp\left[(z-1)\sqrt{s^2+a^2/4H_S^2}\right] \right. \\ & \left. - F(a',b';c';u) F(1+a'-c', 1+b'-c'; 2-c'; -\beta) \exp\left[-(z+1)\sqrt{s^2+a^2/4H_S^2}\right] \right\}, \end{aligned} \tag{3.6}$$

if $0 \le z \le 1$.

$$\begin{aligned} W(z,s) = {} & \frac{\rho_* \exp[(z-2)a/(2H_S)]}{2\rho_0(2a)(1+\beta e^{-2a/D})^{1+D/H_S}\sqrt{s^2+a^2/4H_S^2}} \quad \frac{F(a',b';c';\zeta)}{F(a',b';c';-\beta)} \\ & \times \left\{ F(a',b';c';-\beta) F(1+a'-c', 1+b'-c'; 2-c'; u) \exp\left[(z-2)\sqrt{s^2+a^2/4H_S^2}\right] \right. \\ & \left. - F(a',b';c';u) F(1+a'-c', 1+b'-c'; 2-c'; -\beta) \exp\left[-(z+2)\sqrt{s^2+a^2/4H_S^2}\right] \right\} \end{aligned}$$

$$- \frac{\rho_* \exp[(z-1)a/(2H_S)]}{2\rho_0(a)(1+\beta e^{-a/D})^{1+D/H_S}\sqrt{s^2+a^2/4H_S^2}} \quad \frac{F(a',b';c';u)}{F(a',b';c';-\beta)}$$
$$\times \left\{ F(a',b';c';-\beta)F(1+a'-c',1+b'-c';2-c';\zeta)\exp\left[-(z-1)\sqrt{s^2+a^2/4H_S^2}\right]\right.$$
$$\left. - F(a',b';c';\zeta)F(1+a'-c',1+b'-c';2-c';-\beta)\exp\left[-(z+1)\sqrt{s^2+a^2/4H_S^2}\right]\right\}, \quad (3.7)$$

if $a \le z \le 2$, and

$$W(z,s) = \frac{\rho_* \exp[(z-2)a/(2H_S)]}{2\rho_0(2a)(1+\beta e^{-2a/D})^{1+D/H_S}\sqrt{s^2+a^2/4H_S^2}} \quad \frac{F(a',b';c';u)}{F(a',b';c';-\beta)}$$
$$\times \left\{ F(a',b';c';-\beta)F(1+a'-c',1+b'-c';2-c';\zeta)\exp\left[-(z-2)\sqrt{s^2+a^2/4H_S^2}\right]\right.$$
$$\left. - F(a',b';c';\zeta)F(1+a'-c',1+b'-c';2-c';-\beta)\exp\left[-(z+2)\sqrt{s^2+a^2/4H_S^2}\right]\right\}$$
$$- \frac{\rho_* \exp[(z-1)a/(2H_S)]}{2\rho_0(a)(1+\beta e^{-a/D})^{1+D/H_S}\sqrt{s^2+a^2/4H_S^2}} \quad \frac{F(a',b';c';u)}{F(a',b';c';-\beta)}$$
$$\times \left\{ F(a',b';c';-\beta)F(1+a'-c',1+b'-c';2-c';\zeta)\exp\left[-(z-1)\sqrt{s^2+a^2/4H_S^2}\right]\right.$$
$$\left. - F(a',b';c';\zeta)F(1+a'-c',1+b'-c';2-c';-\beta)\exp\left[-(z+1)\sqrt{s^2+a^2/4H_S^2}\right]\right\}, \quad (3.8)$$

if $2 \le z$. The parameters a', b' and c' are defined by (B.4)-(B.5). In the limit of $\beta \to 0$ (an isothermal atmosphere), the hypergeometric functions tend to one and we recover Lamb's solution (A.5). During the numerical inversion of (3.6)-(3.8) a numerical algorithm developed by Mayrhofer and Fischer (1994) was employed to compute Gauss' hypergeometric series for moderate values of $|s|$. For large $|s|$, the asymptotic expansion (Luke 1969, Section 7.2) for the series was used.

To obtain $p(z,t)$ and $\theta(z,t)$, we take the Laplace transform of (2.4) and (2.5). The nondimensional, Laplace-transformed form of these equations are

$$s\Theta(z,s) = \frac{\rho_*\theta_0(z)}{\gamma\rho_0(z)T_0(z)}[H(z-1)-H(z-2)] - \frac{a}{\gamma T_*}\frac{d\theta_0}{dz}\,W(z,s) \quad (3.9)$$

and

$$sP(z,s) = H(z-1)-H(z-2)+\frac{a}{\gamma H_S}\frac{\rho_0(z)}{\rho_*}\,W(z,s) - \frac{\rho_0(z)c^2}{\rho_* c_*^2}\,\frac{dW(z,s)}{dz}. \quad (3.10)$$

All of the transforms were inverted numerically using Talbot's method (Murli and Rizzardi, 1990), except for those terms when the inverse could be obtained by inspection.

To illustrate our solution I first found the T_* for a given β which gave a surface temperature near 288 K. Because T_* decreases with β, so does H_S and a/H_S increases. These values are summarized in Table 1.

For a given β and a/H_S I then computed the energetics for large t. Only the available potential and elastic energies are nonzero and they are given in Table 1. The case of $\beta = 0$ provided a check on the code. As this table shows, as β increases the available potential energy decreases while the available elastic increases. Taken together, their sum decreases with a corresponding increase in the amount of transients. This is shown in Fig. 3. Although there are very slight changes in the locations of the maxima and minima, the evolution of the various energies follows the life cycle found in the Lamb problem.

To understand these slight changes I have plotted the vertical velocity at various times in Fig. 4. As one might expect, differences in the local speed of sound has affected the propagation of the various wave fronts, resulting in slight changes in the exact placement of the maxima and minima in the energetics diagram. On the other hand, we can identity the same progression of wave pulses regardless of the value of β.

Having found the effect that continuous stratification has on hydrostatic adjustment, let us look at the limiting case when the stratification is concentrated in a discontinuity.

4. Two-Level Model

As counterpoint to the results presented in the previous section where the basic state's temperature decreased exponentially from $T_*(1+\beta)$ to T_*, we now examine hydrostatic adjustment in a two-level atmosphere consisting of an isothermal troposphere at temperature T_1 (or scale height H_1) and depth H which lies underneath an infinitely deep, isothermal stratosphere at temperature T_* (or scale height H_S). Because each layer is isothermal, (2.2)–(2.5) still holds in each layer. However, the basic state is now given by

$$p_0(z) = \begin{cases} p_* e^{-z/H_1}, & 0 \le z \le H \\ p_* e^{-H/H_1-(z-H)/H_S}, & H \le z, \end{cases} \qquad \theta_0(z) = \begin{cases} T_1 e^{\kappa z/H_1}, & 0 \le z \le H \\ T_* e^{\kappa z/H_S+\kappa H/H_1}, & H \le z, \end{cases} \tag{4.1}$$

and

$$\rho_0(z) = \begin{cases} \rho_* T_* e^{-z/H_1}/T_1, & 0 \le z \le H \\ \rho_* e^{-H/H_1-(z-H)/H_S}, & H \le z, \end{cases} \tag{4.2}$$

Using the same nondimensionalization as in Section 2, I show in Appendix C that the Laplace transform of the nondimensional velocity is

$$W_1(z,s) = \tfrac{1}{2} e^{az/2H_1} \left[e^{a/H_1} W_1(z,s|2) - e^{a/2H_1} W_1(z,s|1) \right] \tag{4.3}$$

and

$$W_2(z,s) = e^{az/2H_S}\left[e^{a/H_1}W_2(z,s|2) - e^{a/2H_1}W_2(z,s|1)\right]. \tag{4.4}$$

where

$$\begin{aligned} W_1(z,s|z_s) = {} & e^{-\mu_1|z-z_s|}/\mu_1 - e^{-\mu_1(z+z_s)}/\mu_1 \\ & - \left[e^{-\mu_1|z-z_s|} + e^{\mu_1|z-z_s|} - e^{-\mu_1(z+z_s)} - e^{\mu_1(z+z_s)}\right] \\ & \times \left[Ae^{-2\mu_1 H/a} - A^2e^{-4\mu_1 H/a} + A^3e^{-6\mu_1 H/a} - \ldots\right]/\mu_1 \end{aligned} \tag{4.5}$$

for $0 \le z \le H/a$,

$$e^{H/2H_S - H/2H_1}W_2(z,s|z_s) = \frac{e^{-\mu_1(H/a-z_s)} - e^{-\mu_1(H/a+z_s)}}{\mu_1+\mu_2-\alpha}\left[Ae^{-2\mu_1 H/a} - A^2e^{-4\mu_1 H/a} + A^3e^{-6\mu_1 H/a} - \ldots\right] \tag{4.6}$$

for $H/a \le z$,

$$A = \frac{\mu_1-\mu_2+\alpha}{\mu_1+\mu_2-\alpha}, \qquad \text{and} \qquad \alpha = \left(\frac{a}{2H_S} - \frac{a}{\gamma H_S}\right)\left(1 - \frac{H_S}{H_1}\right). \tag{4.7}$$

The variable μ_i is given in (C.7) with the restriction that $\mathrm{Re}(\mu_2) \ge 0$. We may compute $\Theta(z,s)$ and $P(z,s)$ from (3.9)-(3.10).

Equation (4.3)-(4.7) provide a clear physical picture of the wave field. The first term in (4.5) represents the direct wave excited at $z = z_s$. Waves radiate both upward and downward. The downward propagating waves eventually reflect at the earth's surface and then propagate upward. This process is given by the second term in (4.5).

When a direct or reflected wave reaches the tropopause, a portion is reflected back into the troposphere [the term given by $Ae^{-2\mu_1 H/a}$ in (4.5)] and some of the energy escapes into the stratosphere [the term given by $Ae^{-2\mu_1 H/a}$ in (4.6)]. The waves that are reflected by the tropopause propagate down to the earth's surface where they are reflected. These reflected waves again propagate to the tropopause where some of the energy is reflected and some escapes. Thus the terms given by $A^n e^{-2n\mu_1 H/a}$ in (4.5) represents the internal reflections within the tropospheric waveguide while the corresponding terms in (4.6) represent the continual bleeding of energy out of the troposphere. Eventually all of the transients escape, leaving the hydrostatically adjusted basic state. Because these modes represent the leakage of wave energy away from the troposphere, we shall refer to them as "leaky modes".

To illustrate our results I have computed solutions when the tropospheric temperature is 290 K and the stratospheric temperature is 150 and 220 K. Although 220 K is a realistic temperature for the stratosphere, 150 K is too cold. My reason for including this case is to see what happens when the temperature contrast across the tropopause is very strong. As in the previous sections, Talbot's method was used to numerically invert the Laplace transform term by term.

Figure 5 shows the temporal evolution of the kinetic (KE), available potential (PE) and available elastic (AE) energies for the stratospheric temperatures of 290, 220 and 150 K. The tropospheric temperature is maintained at 290 K. As this figures shows, until the wave front reaches the tropopause, the temporal evolution is the same, regardless of stratospheric temperature. The differences in the curves of AE and PE are due to different values of steady-state AE and PE. Table 2 gives these steady-state values and shows that they increase with a decrease in stratospheric temperature.

The general evolution of the KE, PE and AE is very similar to the Lamb problem. However, as the stratospheric temperature decreases, several additional and shorter period oscillations develop: this is especially evident in the plot of kinetic energy. These additional undulations are due to the reflections within the tropospheric waveguide and the subsequent release of energy into the stratosphere on a later reflection.

To examine how the presence of a strong tropopause affects the actual wave solutions I have graphed the nondimensional vertical velocities at various nondimensional times $c_1 t/a$, where c_1 is the speed of sound in the tropospheric layer. Figure 6 shows these results when the stratospheric temperature is 290 and 150 K. The effect of the colder stratosphere is two-fold: First, wave solutions that propagate into the stratosphere travel at a slower speed. This is quite reasonable because the temperature and speed of the sound are lower there. Second we see multiple reflections in the amplitude of the vertical velocity from reflections off the tropopause.

5. Conclusions

The effects of stratification on hydrostatic adjustment arising from tropospheric diabatic heating have been examined. These are the key finding:

- To a good approximation, hydrostatic adjustment in a stratified atmosphere is similar to that in an

isothermal atmosphere: Initially acoustic waves are generated with the kinetic energy growing or decaying at the expense the available elastic energy. Within two oscillations the acoustic waves evolve into acoustic-gravity waves. Hydrostatic adjustment occurs during the next 3 to 4 oscillations.

• In an atmosphere with continuous stratification, the primary effect of the stratification is on the shape and amplitude of the disturbances as differences in the local speed of sound accelerate and retard propagation.

• In an atmosphere with a sharp tropopause, small, but distinct, reflections may be observed. These internally reflecting waves trap a small amount of the energy within the tropospheric waveguide. Eventually all of the transients are able to escape and radiate out to infinity.

Appendix A

We begin our solution of (2.10) by first introducing the nondimensional variables $z' = z/a$, $t' = ct/a$ and $w' = w/\Delta w$. Dropping the primes, we have that

$$\frac{\partial^2 w}{\partial t^2} + \frac{a}{H_S}\frac{\partial w}{\partial z} - \frac{\partial^2 w}{\partial z^2} = -\frac{\rho_*}{\rho_0}[\delta(z-1) - \delta(z-2)]\delta(t). \tag{A.1}$$

Taking the Laplace transform of (A.1), we find that

$$\frac{d^2\mathcal{W}}{dz^2} - \left(s^2 + \frac{a^2}{4H_S^2}\right)\mathcal{W} = e^{a/2H_S}\delta(z-1) - e^{a/H_S}\delta(z-2), \tag{A.2}$$

where $W(z,s) = e^{az/2H_S}\mathcal{W}(z,s)$. To solve (A.2), we use Fourier sine transforms. We have chosen this particular transform because it ensures that $w(0,t) = 0$ for all t. Upon applying this transform, we obtain

$$\overline{\mathcal{W}}(k,s) = \frac{\sin(2k)e^{a/H_S} - \sin(k)e^{a/2H_S}}{k^2 + s^2 + a^2/4H_S^2}. \tag{A.3}$$

Consequently,

$$\mathcal{W}(z,s) = \frac{2}{\pi}\int_0^\infty \frac{\sin(2k)e^{a/H_S} - \sin(k)e^{a/2H_S}}{k^2 + s^2 + a^2/4H_S^2}\sin(kz)\,dk \tag{A.4}$$

$$= \frac{e^{a/H_S}}{2\sqrt{s^2 + a^2/4H_S^2}}\left[e^{-|z-2|\sqrt{s^2+a^2/4H_S^2}} - e^{-(z+2)\sqrt{s^2+a^2/4H_S^2}}\right]$$

$$- \frac{e^{a/2H_S}}{2\sqrt{s^2 + a^2/4H_S^2}}\left[e^{-|z-1|\sqrt{s^2+a^2/4H_S^2}} - e^{-(z+1)\sqrt{s^2+a^2/4H_S^2}}\right]. \tag{A.5}$$

where we have evaluated (A.4) using integral tables (Gradshteyn and Ryzhik 1965, formula 3.742.1). Because

$$\mathcal{L}^{-1}\left[\frac{\exp(-b\sqrt{s^2+a^2})}{s^2+a^2}\right] = J_0\left(a\sqrt{t^2-b^2}\right)H(t-b), \quad b > 0, \tag{A.6}$$

we obtain (2.11) from (A.5).

To compute $p(z,t)$ and $\theta(z,t)$, we take the Laplace transform of (2.4) and (2.5) and find that

$$P(z,s) = \frac{H(z-1) - H(z-2)}{s}$$

$$+ \tfrac{1}{2}e^{a/H_S}e^{-az/2H_S}\left[\mathrm{sgn}(z-2)\frac{e^{-|z-2|\sqrt{s^2+a^2/4H_S^2}}}{s} - \frac{e^{-(z+2)\sqrt{s^2+a^2/4H_S^2}}}{s}\right]$$

$$- \tfrac{1}{2}e^{a/2H_S}e^{-az/2H_S}\left[\mathrm{sgn}(z-1)\frac{e^{-|z-1|\sqrt{s^2+a^2/4H_S^2}}}{s} - \frac{e^{-(z+1)\sqrt{s^2+a^2/4H_S^2}}}{s}\right]$$

$$- \frac{(\gamma-2)ae^{a/H_S}e^{-az/2H_S}}{4\gamma H_S s\sqrt{s^2+a^2/4H_S^2}}\left[e^{-|z-2|\sqrt{s^2+a^2/4H_S^2}} - e^{-(z+2)\sqrt{s^2+a^2/4H_S^2}}\right]$$

$$+ \frac{(\gamma-2)ae^{a/2H_S}e^{-az/2H_S}}{4\gamma H_S s\sqrt{s^2+a^2/4H_S^2}}\left[e^{-|z-1|\sqrt{s^2+a^2/4H_S^2}} - e^{-(z+1)\sqrt{s^2+a^2/4H_S^2}}\right] \tag{A.7}$$

and

$$\Theta(z,s) = e^{(1+\kappa)az/H_S}\frac{H(z-1)-H(z-2)}{\gamma s} - \frac{\kappa a e^{a/H_S}e^{(1+2\kappa)az/2H_S}}{2\gamma H_S s\sqrt{s^2+a^2/4H_S^2}}\left[e^{-|z-2|\sqrt{s^2+a^2/4H_S^2}} - e^{-(z+2)\sqrt{s^2+a^2/4H_S^2}}\right] + \frac{\kappa a e^{a/2H_S}e^{(1+2\kappa)az/2H_S}}{2\gamma H_S s\sqrt{s^2+a^2/4H_S^2}}\left[e^{-|z-1|\sqrt{s^2+a^2/4H_S^2}} - e^{-(z+1)\sqrt{s^2+a^2/4H_S^2}}\right]. \quad \textbf{(A.8)}$$

To find $p(z,t)$ and $\theta(z,t)$, we must invert two transforms:

$$F(s) = \frac{e^{-b\sqrt{s^2+a^2}}}{s} \quad \text{and} \quad G(s) = \frac{e^{-b\sqrt{s^2+a^2}}}{s\sqrt{s^2+a^2}}, \qquad b>0. \quad \textbf{(A.9)}$$

To invert $F(s)$, we note that

$$e^{-bs} - e^{-b\sqrt{s^2+a^2}} = ab\,\mathcal{L}\left[\frac{J_1(a\sqrt{t^2-b^2})}{\sqrt{t^2-b^2}}H(t-b)\right] \quad \textbf{(A.10)}$$

or

$$\frac{e^{-bs}}{s} - \frac{e^{-b\sqrt{s^2+a^2}}}{s} = ab\,\mathcal{L}\left[H(t-b)\int_b^t \frac{J_1(a\sqrt{\tau^2-b^2})}{\sqrt{\tau^2-b^2}}\,d\tau\right] \quad \textbf{(A.11)}$$

so that

$$\mathcal{L}^{-1}\left(\frac{e^{-b\sqrt{s^2+a^2}}}{s}\right) = H(t-b)\left[1 - ab\int_b^t \frac{J_1(a\sqrt{\tau^2-b^2})}{\sqrt{\tau^2-b^2}}\,d\tau\right]. \quad \textbf{(A.12)}$$

In a similar manner,

$$\mathcal{L}^{-1}\left(\frac{e^{-b\sqrt{s^2+a^2}}}{s\sqrt{s^2+a^2}}\right) = H(t-b)\int_b^t J_0\left(a\sqrt{\tau^2-b^2}\right)\,d\tau. \quad \textbf{(A.13)}$$

Appendix B

We begin our solution by introducing $W(z,s) = e^{a\nu z/H_S}\mathcal{W}(z,s)$. Eq. (3.5) then becomes

$$\left(1+\beta e^{-az/D}\right)\left(\frac{d^2\mathcal{W}}{dz^2} + \frac{2a\nu}{H_S}\frac{d\mathcal{W}}{dz} + \frac{a^2\nu^2}{H_S^2}\mathcal{W}\right) - \frac{a}{H_S}\left(\frac{d\mathcal{W}}{dz} + \frac{a\nu}{H_S}\mathcal{W}\right) - s^2\mathcal{W} = \frac{\rho_*}{\rho_0(z)}e^{-a\nu z/H_S}[\delta(z-1)-\delta(z-2)]. \quad \textbf{(B.1)}$$

We now introduce the new independent variable $u = -\beta e^{-az/D}$. Equation (B.1) becomes

$$(1-u)u\frac{d^2\mathcal{W}}{du^2} + [c' - (1-a'-b')u]\frac{d\mathcal{W}}{du} - a'^2b'^2\mathcal{W} = \frac{D^2\rho_*}{a^2\rho_0(u)}\frac{u^{\nu D/H_S-1}}{(-\beta)^{\nu D/H_S}}[\delta(u-u_1)-\delta(u-u_2)]. \quad \textbf{(B.2)}$$

where

$$\nu = \frac{1}{2} - \frac{1}{2}\sqrt{1 + \frac{4s^2 H_S^2}{a^2}} \ . \tag{B.3}$$

$$a' = b' = -\frac{D}{2H_S}\left(1 - \sqrt{1 + \frac{4s^2 H_S^2}{a^2}}\right) . \tag{B.4}$$

$$c' = 1 + \frac{D}{H_S}\sqrt{1 + \frac{4s^2 H_S^2}{a^2}} \ , \tag{B.5}$$

and u_i denote the value of u corresponding to z_i.

Our particular choice of ν was motivated by two factors. First, this choice yields the classic Gauss hypergeometric equation. Second, we anticipate that the solution for the exponential temperature profile should be very similar to Lamb's solution. After all, the temperature profile differs markedly only near the ground. If we choose the ν given by (B.3), then e^{az/H_S} becomes the Lamb solution and $W(z,s)$ is merely the correction arising from the $e^{-az/D}$ term in the temperature profile.

Consider the differential equation

$$(1-u)u\frac{d^2g}{du^2} + [c' - (1 - a' - b')u]\frac{dg}{du} - a'^2 b'^2 g = -\delta(u - \zeta). \tag{B.6}$$

With the requirement that $g(-\beta|\zeta) = 0$,

$$g(u|\zeta) = \begin{cases} C_1[F(a',b';c';u)G(a',b',c';-\beta) - F(a',b',c';-\beta)G(a',b';c';u)], & -\beta \le u \le \zeta, \\ C_2 F(a',b';c';u), & \zeta \le u \le 0. \end{cases} \tag{B.7}$$

where $F(a',b';c';u)$ and $G(a',b';c';u)$ are hypergeometric functions of the first and second kind, respectively. See Lebedev (1972, Chapter 9). The arbitrary constants C_1 and C_2 are found by requiring that

$$\lim_{u\to\zeta^-} g(u|\zeta) = \lim_{u\to\zeta^+} g(u|\zeta) \qquad \text{and} \qquad (1-u)u\frac{dg}{du}\bigg|_{\zeta^-}^{\zeta^+} = -1. \tag{B.8}$$

The second condition in (B.8) follows from integrating (B.6) over the infinitesimally thin interval $[\zeta^-, \zeta^+]$, where ζ^- and ζ^+ denote points just below and above the point $u = \zeta$. These relationships yield

$$C_1 = \frac{\Gamma(a')\Gamma(b')F(a',b';c';\zeta)}{\Gamma(c')\zeta^{1-c'}(1-\zeta)^{c'-a'-b'}F(a',b';c';-\beta)} \tag{B.9}$$

and

$$C_2 = \frac{\Gamma(a')\Gamma(b')[F(a',b';c';\zeta)G(a',b',c';-\beta) - F(a',b',c';-\beta)G(a',b';c';\zeta)]}{\Gamma(c')\zeta^{1-c'}(1-\zeta)^{c'-a'-b'}F(a',b';c';-\beta)}. \tag{B.10}$$

where $\Gamma(\ )$ is the gamma function (Lebedev, 1972, Chapter 1). In deriving (B.9) (B.10) we have used the properties of the Wronskian as they apply to hypergeometric functions (Lebedev, 1972, p. 278, problem 9). Substituting of C_1 and C_2 into (B.7) yields

$$g(u|\zeta) = \frac{(-\beta)^{1-c'}F(a',b';c';u)F(1+a'-c',1+b'-c',2-c';-\beta)F(a',b';c';\zeta)}{(c'-1)\zeta^{1-c'}(1-\zeta)^{c'-a'-b'}F(a',b';c';-\beta)} - \frac{u^{1-c'}F(a',b',c';-\beta)F(1+a'-c',1+b'-c';2-c';u)F(a',b';c';\zeta)}{(c'-1)\zeta^{1-c'}(1-\zeta)^{c'-a'-b'}F(a',b';c';-\beta)}, \qquad \textbf{(B.11)}$$

if $-\beta \le u \le \zeta$, and

$$g(u|\zeta) = \frac{(-\beta)^{1-c'}F(a',b';c';\zeta)F(1+a'-c',1+b'-c',2-c';-\beta)F(a',b';c';u)}{(c'-1)\zeta^{1-c'}(1-\zeta)^{c'-a'-b'}F(a',b';c';-\beta)} - \frac{\zeta^{1-c'}F(a',b',c';-\beta)F(1+a'-c',1+b'-c';2-c';\zeta)F(a',b';c';u)}{(c'-1)\zeta^{1-c'}(1-\zeta)^{c'-a'-b'}F(a',b';c';-\beta)}, \qquad \textbf{(B.11)}$$

if $\zeta \le u \le 0$. To derive (B.11)–(B.12) we used the relationships that $\Gamma(c')/\Gamma(c'-1) = c'-1$ and the relationship between $G(a',b',c';z)$ and $F(a',b',c';z)$ (Lebedev, 1972, p. 277, problem 7). The final solution is obtained by substituting for a', b' and c', applying the results to each of the impulsive forcings in (B.2) and multiplying by the appropriate coefficients.

Our ability to express $G(a',b';c';z)$ in terms of $F(a',b';c';z)$ and $F(1+a'-c',1+b'-c';2-c';z)$ requires that the contour of integration not pass near the singularities $c' = 0, \pm 1, \pm 2, \ldots$. When the contour generated by the numerical inversion did, we took an equivalent contour [increased λ as suggested by Murli and Rizzardi (1990)] to avoid coding this special case.

Appendix C

We begin our analysis by taking the Laplace transform of (2.10). Because of the linearity of the problem, we only have to solve an equation of the form

$$\frac{H_S}{H_1}\frac{\partial^2 w_1}{\partial t^2} + \frac{a}{H_1}\frac{\partial w_1}{\partial z} - \frac{\partial^2 w_1}{\partial z^2} = -\frac{H_S \rho_s}{H_1 \rho_0(z_s)}\delta(z-z_s)\delta(t) \quad \text{for} \quad 0 \le z \le H/a \qquad \textbf{(C.1)}$$

and

$$\frac{\partial^2 w_2}{\partial t^2} + \frac{a}{H_S}\frac{\partial w_2}{\partial z} - \frac{\partial^2 w_2}{\partial z^2} = 0 \qquad \text{for} \qquad H/a \le z. \qquad \textbf{(C.2)}$$

To find the solution for (2.10) we then subtract the solution for $z_s = 2$ from the one for $z_s = 1$. Again I have scaled the vertical distance with a and time with a/c_*. Denoting the transform of the nondimensional vertical velocity by $W_1(z,s)$, we have that

$$\frac{d^2W_1}{dz^2} - \left(\frac{H_S}{H_1}s^2 + \frac{a^2}{4H_1^2}\right)W_1 = e^{-az_s/2H_1}\frac{H_S\rho_*}{H_1\rho_0(z_s)}\delta(z - z_s) \tag{C.3}$$

for the troposphere and

$$\frac{d^2W_2}{dz^2} - \left(s^2 + \frac{a^2}{4H_S^2}\right)W_2 = 0 \tag{C.4}$$

for the stratosphere, where $W_1(z,s) = e^{az/2H_1}\mathcal{W}_1(z,s)$ and $W_2(z,s) = e^{az/2H_S}\mathcal{W}_2(z,s)$.

Taking $w_1(0,t) = 0$ and the radiation boundary condition into account, the solutions to (C.3)–(C.4) are

$$\mathcal{W}_1(z,s) = \begin{cases} A\sinh(\mu_1 z), & 0 \le z \le z_s \\ B\sinh(\mu_1 z) + C\cosh(\mu_1 z), & z_s \le z \le H/a \end{cases} \tag{C.5}$$

and

$$\mathcal{W}_2(z,s) = D\exp[-\mu_2(z - H/a)], \tag{C.6}$$

where

$$\mu_1^2 = \frac{H_S}{H_1}s^2 + \frac{a^2}{4H_1^2} \qquad \text{and} \qquad \mu_2^2 = s^2 + \frac{a^2}{4H_S^2}. \tag{C.7}$$

Here we have chosen the branch $\mathrm{Re}(\mu_2) \ge 0$. The remaining task is to find A, B, C and D. The kinematic boundary condition leads to $\mathcal{W}_1(H,s) = \widehat{\mathcal{W}}_2(H,s)$, where $\widehat{\mathcal{W}}_2(z,s) = e^{H/2H_S - H/2H_1}\mathcal{W}_2(z,s)$. A combination of the dynamic and kinematic boundary conditions applied to the Laplace transformed (2.4) yields the second condition that

$$\frac{d\mathcal{W}_1(H,s)}{dz} = \frac{d\widehat{\mathcal{W}}_2(H,s)}{dz} + \left(\frac{a}{2H_S} - \frac{a}{\gamma H_S}\right)\left(1 - \frac{H_S}{H_1}\right)\widehat{\mathcal{W}}_2(H,s). \tag{C.8}$$

At the point of singularity, continuity of the solution requires that $\mathcal{W}_1(z_s^-,s) = \mathcal{W}_1(z_s^+,s)$, where z_s^- and z_s^+ denote points just below and above $z = z_s$, respectively. Finally, an integration of (C.3) over the interval $[z_s^-, z_s^+]$ yields the final condition that

$$\left.\frac{d\mathcal{W}_1}{dz}\right|_{z_s^-}^{z_s^+} = e^{-az_s/2H_1}\frac{H_S\rho_*}{H_1\rho_0(z_s)}. \tag{C.9}$$

Substituting (C.5)–(C.6) into these four conditions gives the solutions listed in Section 4, except in terms of hyperbolic cosines and sines. Finally we express the hyperbolic functions in terms of exponentials and expand the denominator as a geometric series in $e^{-2\mu_1 H/a}$.

References

Bannon, P. R., 1995: Hydrostatic adjustment: Lamb's problem. *J. Atmos. Sci.*, **52**, 1743–1752.

Francis, S. H., 1973: Acoustic-gravity modes and large-scale traveling ionospheric disturbances of a realistic, dissipative atmosphere. *J. Geophys. Res.*, **71**, 1033–1054.

Fröberg, C.-E., 1969: *Introduction to Numerical Analysis*. Addison-Wesley Publishing Co., 433 pp.

Friedman, J. P., 1966: Propagation of internal gravity waves in a thermally stratified atmosphere. *J. Geophys. Res.*, **71**, 1033–1054.

Gradshteyn, I. S., and I. M. Ryzhik, 1965: *Table of Integrals, Series, and Products*. Academic Press, 1086 pp.

Lebedev, N. N., 1972: *Special Functions and Their Applications*, Dover Publications, 308 pp.

Luke, Y. L., 1969: *The Special Functions and Their Applications*. Academic Press, 349 pp.

Mayrhofer, K., and F. D. Fischer, 1994: Analytical solutions and a numerical algorithm for the Gauss's hypergeometric function ${}_2F_1(a,b;c;z)$. *Zeit. Angew. Math. Mech.*, **74**, 265–273.

Murli, A., and M. Rizzardi, 1990: Algorithm 682: Talbot's method for the Laplace inversion. *ACM Trans. Math. Softw.*, **16**, 158–168.

Pekeris, C. L., 1948: The propagation of a pulse in the atmosphere. Part II. *Phys. Review*, **73**, 145–154.

Rossby, C. G., 1938: On the mutual adjustment of pressure and velocity distributions in certain simple current systems. *J. Mar. Res.*, **1**, 15–28, 239–263.

Stone, P. H., 1978: Baroclinic adjustment. *J. Atmos. Sci.*, **35**, 561–571.

Tables

Table 1: Distribution of available potential (PE) and available elastic (AE) energies in the final equilibrium state in an nonisothermal atmosphere where the temperature behaves according to (3.1) with $D/H_S = 1.5$. The percentages give the ratio of the corresponding energy to the total energy.

β	T_*	$T_0(0)$	a/H_S	PE	AE
0.0	290 K	290 K	0.500	64.74%	6.71%
0.1	260 K	288 K	0.558	60.58%	8.32%
0.2	240 K	286 K	0.604	56.92%	9.79%
0.3	220 K	286 K	0.659	53.57%	11.39%

Table 2: Same as Table 1 except for a two-level atmosphere with $a/H_S = 0.5$.

Tropospheric Temperature	Stratospheric Temperature	PE	AE
290 K	290 K	64.74%	6.71%
290 K	220 K	65.55%	7.35%
290 K	150 K	66.69%	8.39%

Tables

Table 1: Distribution of available potential (PE) and available elastic (AE) energies in the final equilibrium state in an nonisothermal atmosphere where the temperature behaves according to (3.1) with $D/H_S = 1.5$. The percentages give the ratio of the corresponding energy to the total energy.

β	T_*	$T_0(0)$	a/H_S	PE	AE
0.0	290 K	290 K	0.500	64.74%	6.71%
0.1	260 K	288 K	0.558	60.58%	8.32%
0.2	240 K	286 K	0.604	56.92%	9.79%
0.3	220 K	286 K	0.659	53.57%	11.39%

Table 2: Same as Table 1 except for a two-level atmosphere with $a/H_S = 0.5$.

Tropospheric Temperature	Stratospheric Temperature	PE	AE
290 K	290 K	64.74%	6.71%
290 K	220 K	65.55%	7.35%
290 K	150 K	66.69%	8.39%

Figures

Figure 1: The transient portion of available elastic (AE), available potential (PE) and kinetic (KE) energies in terms of the percentage of total energy as a function of nondimensional time ct/a. The solid line gives the case when $a/H_S = 0.25$ while the dashed line corresponds to $a/H_S = 0.5$.

Figure 2: The variation of integrand of (2.19) corresponding to the the available elastic (AE), available potential (PE) and kinetic (KE) energies as a function of nondimensional distance z/a at the nondimensional times of $ct/a = 10$ (solid line), 25 (dashed line) and 50 (dot-dashed line). The parameter $a/H_S = 0.5$.

Figure 3: Same as Figure 1 except for an atmosphere with a basic state temperature given by (3.1). The solid line gives the isothermal case when $T_* = 290$ K and $\beta = 0$ while the dashed and long dashed lines correspond to $T_* = 250$ K, $\beta = 0.15$ and $T_* = 220$ K, $\beta = 0.3$, respectively.

Figure 4: The nondimensional vertical velocity in an atmosphere where the basic state temperature is given by (3.1). The solid line gives the isothermal case of $T_* = 290$ K and $\beta = 0$ while the dashed line corresponds to $T_* = 220$ K and $\beta = 0.3$. The corresponding a/H_S are 0.5 and 0.66, respectively. The snapshots are at the nondimensional times ct/a of (a) 1.0, (b) 1.5, (c) 2.0 and (d) 2.5, where c is the speed of sound corresponding to 290 K.

Figure 5: Same as Figure 1 except for a two-level atmosphere. The solid line corresponds to the case when the stratospheric temperature is 290 K; the dashed line, 220 K; and the dash-dotted line, 150 K. In all cases the tropospheric temperature is 290 K. The nondimensional time is now $c_1 t/a$ and $a/H_S = 0.5$, where c_1 is the speed of sound in the troposphere.

Figure 6: Same as Figure 4 except for a two-level atmosphere where the tropospheric temperature is 290 K and the stratospheric temperature is either 290 K (solid line) or 150 K (dashed line). The snapshots are at the nondimensional times $c_1 t/a$ of (a) 1.0, (b) 1.5, (c) 2.0 and (d) 2.5 and $a/H_S = 0.5$, where c_1 is the speed of sound in the troposphere. The tropopause lies at $z/a = 2.827$.

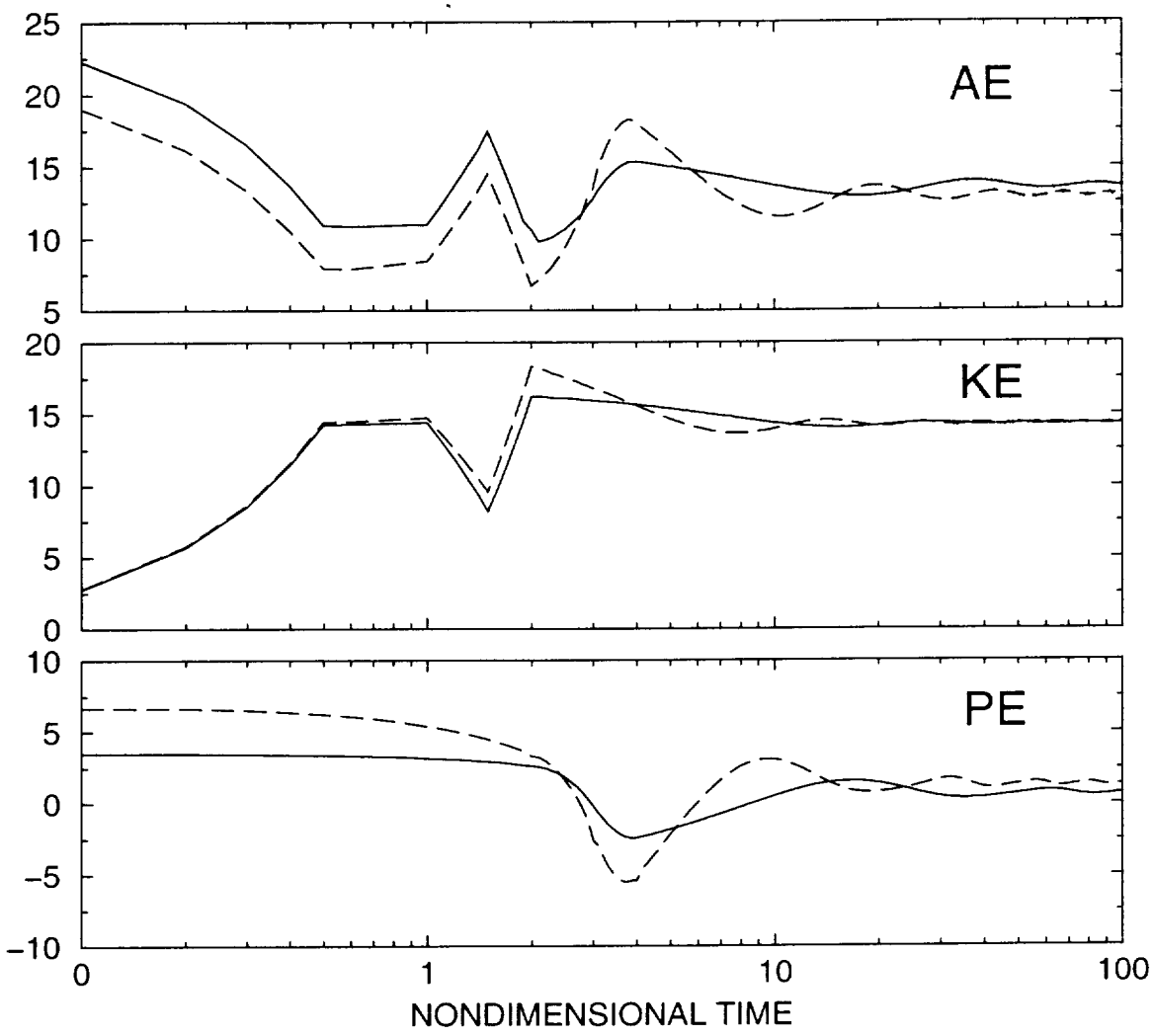

Figure 1: The transient portion of available elastic (AE), available potential (PE) and kinetic (KE) energies in terms of the percentage of total energy as a function of nondimensional time ct/a. The solid line gives the case when $a/H_S = 0.25$ while the dashed line corresponds to $a/H_S = 0.5$.

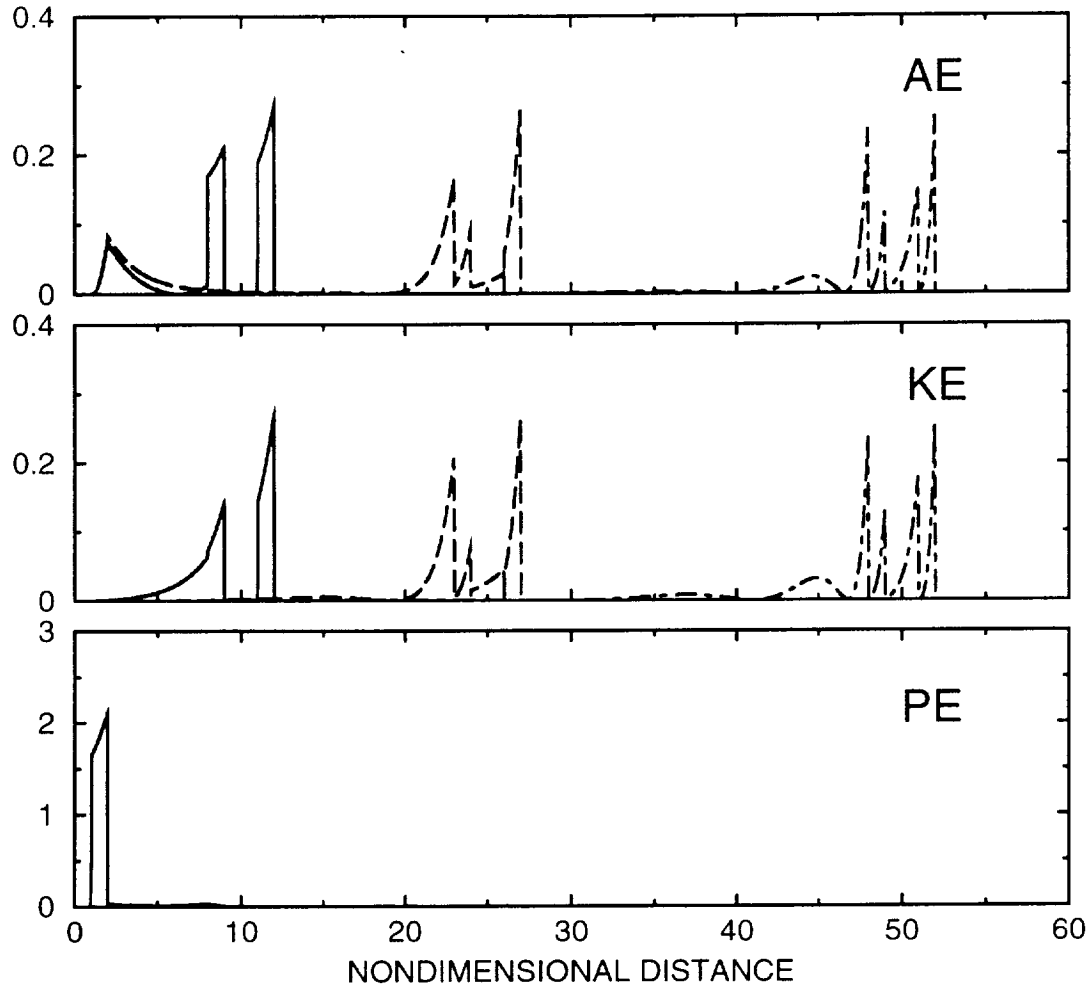

Figure 2: The variation of integrand of (2.19) corresponding to the the available elastic (AE), available potential (PE) and kinetic (KE) energies as a function of nondimensional distance z/a at the nondimensional times of $ct/a = 10$ (solid line), 25 (dashed line) and 50 (dot-dashed line). The parameter $a/H_S = 0.5$.

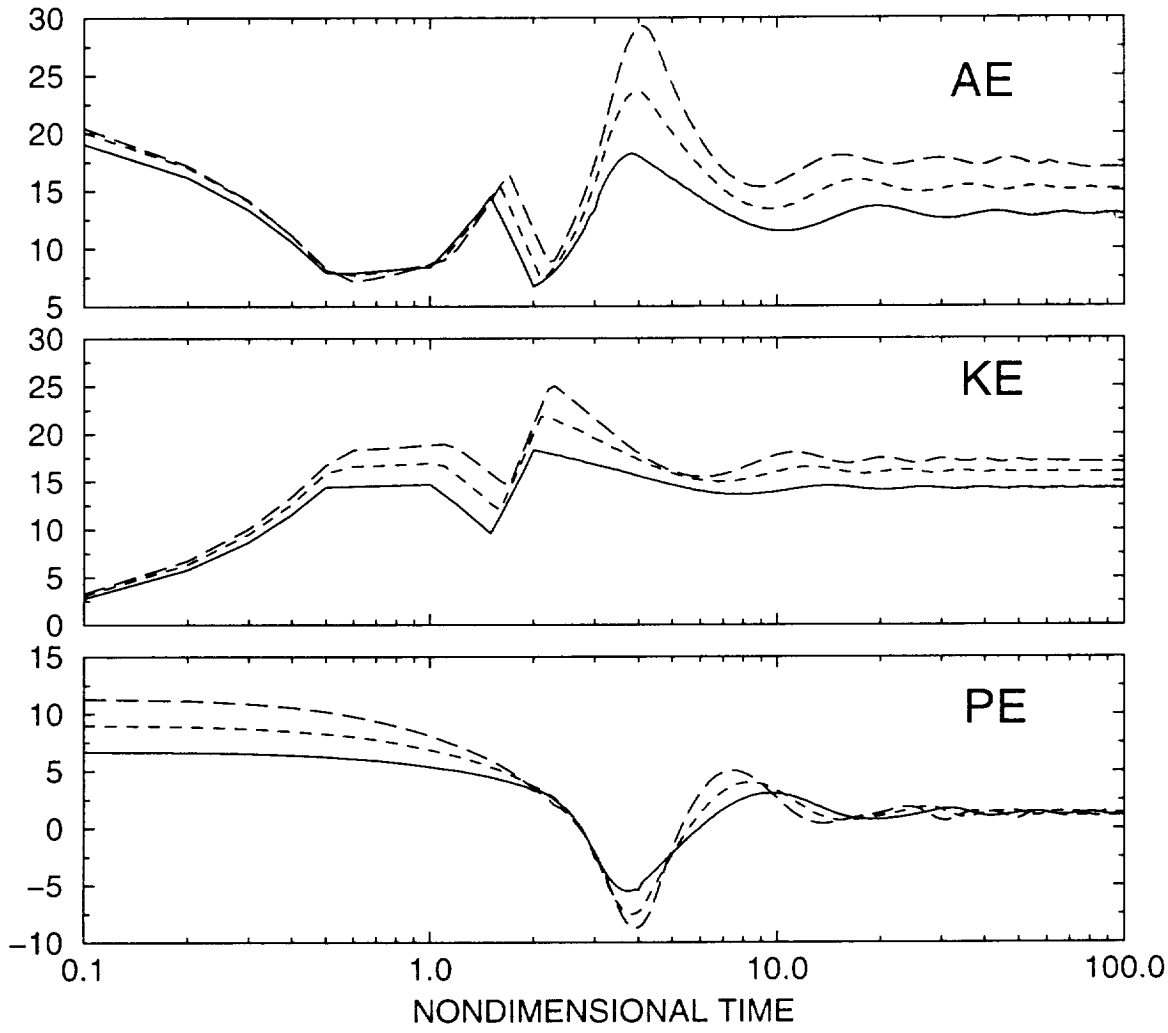

Figure 3: Same as Figure 1 except for an atmosphere with a basic state temperature given by (3.1). The solid line gives the isothermal case when $T_s = 290$ K and $\beta = 0$ while the dashed and long dashed lines correspond to $T_s = 250$ K, $\beta = 0.15$ and $T_s = 220$ K, $\beta = 0.3$, respectively.

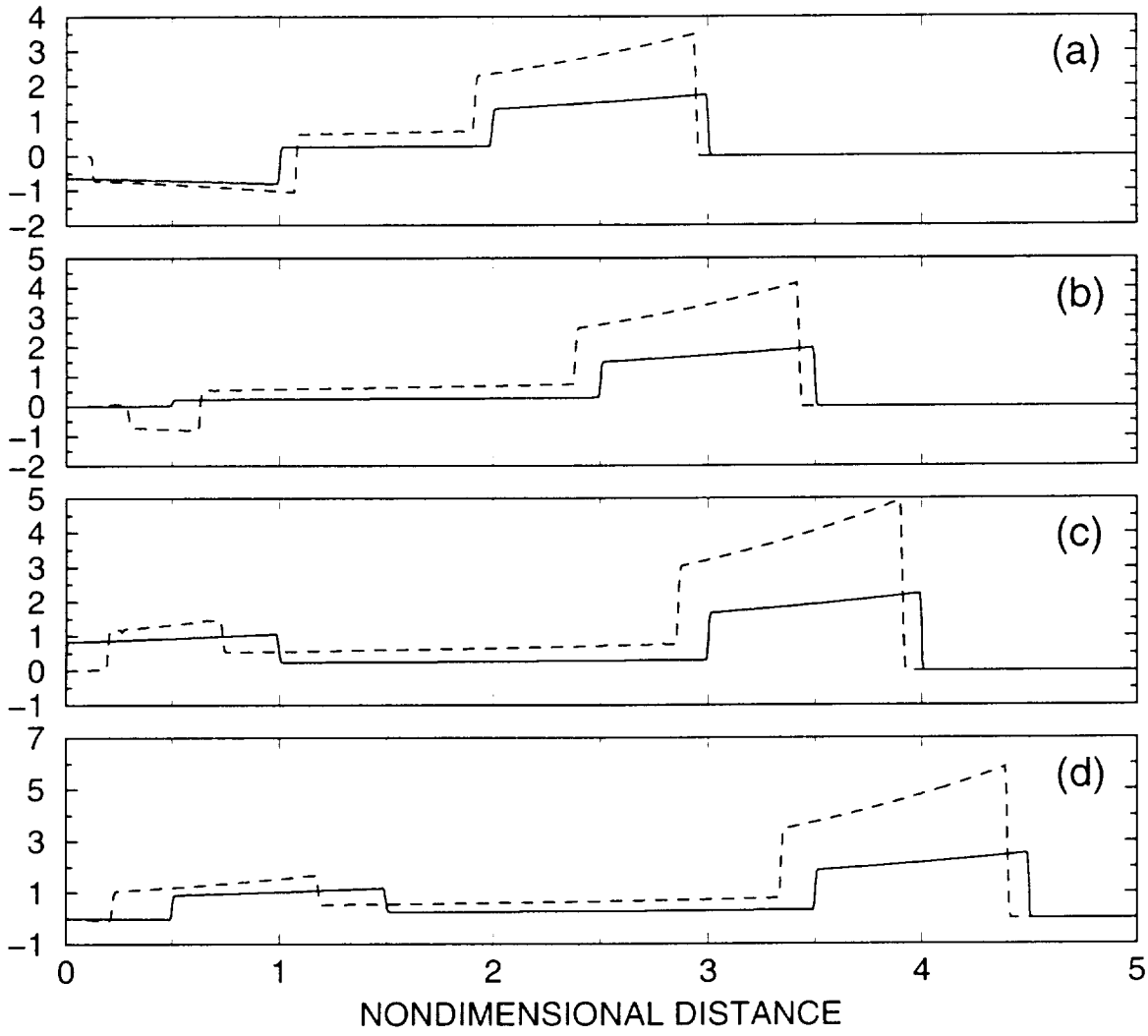

Figure 4: The nondimensional vertical velocity in an atmosphere where the basic state temperature is given by (3.1). The solid line gives the isothermal case of $T_* = 290$ K and $\beta = 0$ while the dashed line corresponds to $T_* = 220$ K and $\beta = 0.3$. The corresponding a/H_S are 0.5 and 0.66, respectively. The snapshots are at the nondimensional times ct/a of (a) 1.0, (b) 1.5, (c) 2.0 and (d) 2.5, where c is the speed of sound corresponding to 290 K.

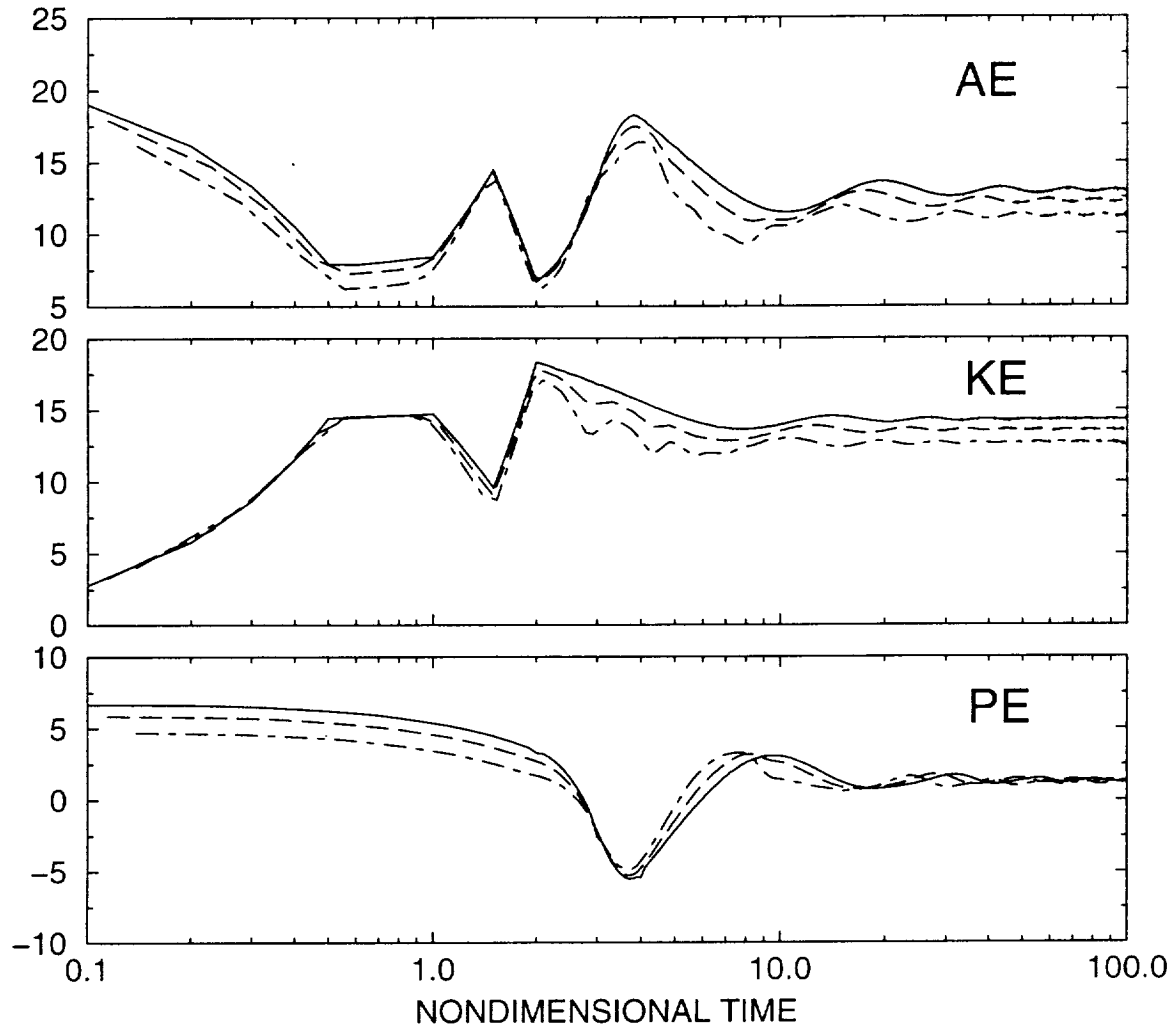

Figure 5: Same as Figure 1 except for a two-level atmosphere. The solid line corresponds to the case when the stratospheric temperature is 290 K; the dashed line, 220 K; and the dash-dotted line, 150 K. In all cases the tropospheric temperature is 290 K. The nondimensional time is now $c_1 t/a$ and $a/H_S = 0.5$, where c_1 is the speed of sound in the troposphere.

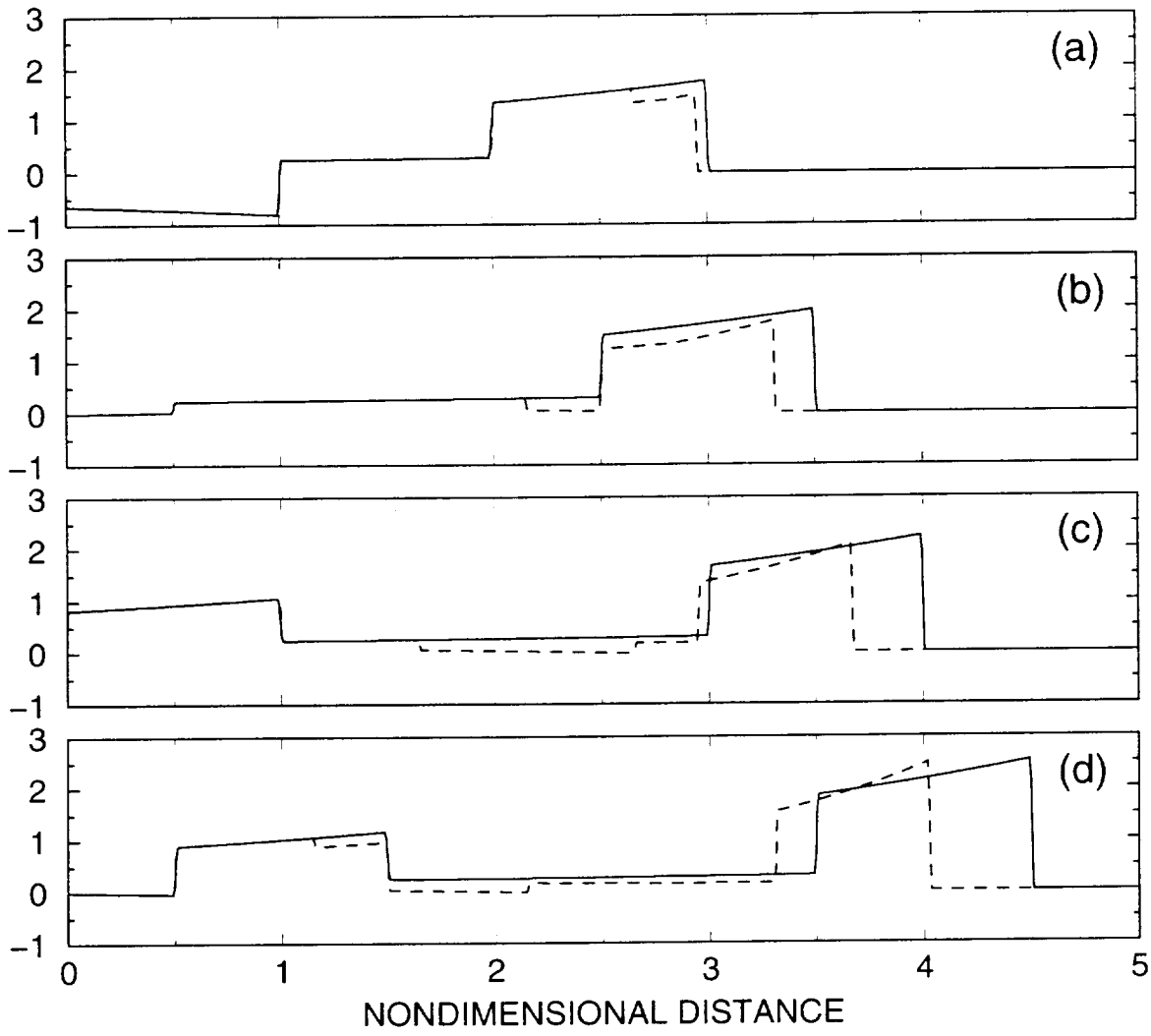

Figure 6: Same as Figure 4 except for a two-level atmosphere where the tropospheric temperature is 290 K and the stratospheric temperature is either 290 K (solid line) or 150 K (dashed line). The snapshots are at the nondimensional times $c_1 t/a$ of (a) 1.0, (b) 1.5, (c) 2.0 and (d) 2.5 and $a/H_S = 0.5$, where c_1 is the speed of sound in the troposphere. The tropopause lies at $z/a = 2.827$.

Popular Summary

The atmosphere is full of waves which differ widely in length and time between peaks. A special group, called acoustic-gravity waves, are generated whenever large pressure differences occur between adjacent chunks of air, such as during earthquakes, developing thunderstorms, and even during the launch of the space shuttle. Although a theory has been constructed of how these waves would propagate out to space if the atmosphere had the same temperature everywhere, this is not very realistic because temperature decreases with altitude. In this paper realistic temperatures are taken into account and it is shown how these variations affect this radiation of energy into space. With the advent of nonhydrostatic models which include these acoustic-gravity waves, this study will hopefully provide tools to better understand these new models.